Brain and behavioral alterations in subjects with social anxiety dominated by empathic embarrassment

Shisei Tei[1], Jukka-Pekka Kauppi, Kathryn F. Jankowski, Junya Fujino, Ricardo P. Monti, Jussi Tohka, Nobuhito Abe, Toshiya Murai, Hidehiko Takahashi[1], Riitta Hari[1]

[1]To whom correspondence may be addressed
Email: chengctky@gmail.com hidepsyc@tmd.ac.jp or riitta.hari@aalto.fi

This PDF file includes:

- Supplementary text
- Figures S1
- Tables S1
- SI References

www.pnas.org/cgi/doi/10.1073/pnas.1918081117

Supplementary Introduction

Our empathic embarrassment setup is based on previous studies that have suggested that empathy may involve affective (bottom-up) and cognitive (top-down) processes (1-3); such that the perceiver would (a) resonate an emotion in the social target via a more dominant affective route (self–other matching) or (b) recognize her own emotion that differs from an emotion in the social target via a more dominant cognitive route (self–other distinction) (2, 4). Accordingly, when an individual encounters a person whose behavior is embarrassing, this individual may empathically acknowledge the situation in two ways, both by sharing the emotion with the person who is embarrassed of herself and aware of her feeling, and by not sharing the emotion with the person whose behavior is embarrassing but this person is unaware of her embarrassment (3).

On this basis, we hypothesized that the EMBAR singers would embarrass the viewer dominantly via affEMP (so that the viewer would share embarrassment with the EMBAR singer) and the PRIDE singers dominantly via cogEMP (so that the viewer would acknowledge the embarrassment of the PRIDE singer). We also predicted that PRIDE singers would trigger stronger cogEMP than affEMP because understanding the embarrassment in a situational context demands dissociating from the PRIDE singer's proud feeling.

Supplementary Methods

Behavioral data

Empathic disposition was assessed using the 28-item Interpersonal Reactivity Index (IRI), which is one of the most widely used self-report measures of dispositional empathy (5). The subscales of personal distress (PD: self-oriented feelings of anxiety and discomfort) and empathic concern (EC: feelings of compassion and concern for others) scores assessed the affective components of empathy, whereas, perspective taking (PT: adopting others' psychological point of view) assessed the cognitive component of empathy (1). Based on previous studies, the fantasy subscale was excluded (6). We assessed subjects' alexithymia level using the 20-item Toronto Alexithymia Scale (TAS-20) (7). Alexithymia represents lack of self-awareness (7), which is a proposed precursor for empathic abnormalities (6, 8). This measure yields three subscales: difficulty in identifying feelings, difficulty in describing feelings, and externally-oriented thinking. In addition, intelligence quotient (IQ) scores were estimated using a Japanese version of the National Adult Reading Test (JART; mean = 104.6 ± 8.35), based on findings from a previous study that demonstrated that JART scores successfully predicted full-scale IQ scores on the Wechsler Adult Intelligence Scale-Revised (9).

We used the Wisconsin Card Sorting Test (WCST), a well-established measure of cognitive flexibility and attentional set-shifting (10), to assess subjects' abilities to switch attention and perspectives. These abilities are crucial for cognitive perspective taking that requires individuals to compare and contrast their own perspectives with those of other people (11, 12). We adopted a computerized version of the WCST (13) where four stimulus cards were displayed on the computer screen. The cards varied according to three perceptual categories: number, color, and shape. Subjects were instructed to select one of the four cards that fit a given perceptual category but they were not told which perceptual category to use. After each card selection, subjects received feedback ('Correct' or 'Incorrect'). The perceptual category used to organize the cards shifted among these three categories during the test until subjects had

selected all 48 cards. We focused on the number of categories achieved (CAs). One CA represented one rule attainment, involving six consecutive correct card selections after a rule change. Therefore, larger CA numbers represented a greater ability to switch attention and decision rules (perspectives) (11). One subject's WCST data were omitted because of a technical error.

fMRI task, data acquisition, and analyses

Subjects watched video clips of female and male singers who were singing badly in front of an audience during a singing competition (Fig. 1). Singers acted embarrassed or proud of their singing [authentic embarrassment (EMBAR) and hubristic pride (PRIDE), respectively]. These performances were designed to embarrass the viewers either via emotion sharing [i.e. affective empathy (affEMP) with EMBAR singers] or via perspective taking [i.e. cognitive empathy (cogEMP) for PRIDE singers]. The setup also included no-singing video clips (singers neither sang nor expressed emotions and listened to instrumental background music) as well as authentic pride video clips (talented singers sang well and expressed proud of their performance). These conditions, comprising six blocks each, similar to EMBAR and PRIDE conditions, will be analyzed using a theoretically and methodologically distinct approach and reported in a separate study.

At single-subject level, we used a GLM in SPM and conducted two *t*-tests for the contrasts EMBAR > PRIDE and EMBAR < PRIDE. The design matrix included task conditions and six movement parameters (three displacements and three rotations). At group level, we conducted ROI-based random-effects analyses to investigate activity specifically recruited within empathy-related brain regions. We selected *a priori* regions that are crucially involved in affective and emotional processing, including e.g. vicarious pain (2). These ROIs included the amygdala, ACC, insula, and vmPFC/OFC. These ROI masks were generated using the Automatic Anatomical Labeling atlas as implemented in the WFU pickatlas toolbox (14). We limited our analysis to the right hemisphere, given that right-hemisphere-dominant brain activity within these hypothesized regions is commonly reported in studies of social cognition (15). Activity within ROI masks was considered statistically significant if it survived FWE correction for multiple comparisons at a cluster-level of $p < 0.01$ (primary threshold at voxel-level uncorrected, $p < 0.001$). Parameter estimates were extracted as first eigenvariates from statistically significant clusters within these *a priori* regions. We also included an ROI in the right pSTS/TPJ likely supporting in cogEMP (16-18). We examined these regions as a single/unified region, in accordance with previous studies (16, 19, 20). Per our previous approach (6), pSTS/TPJ parameter estimates were extracted from a cluster obtained from a whole-brain analysis. Additionally, we reported activity outside these ROIs thresholded at voxel-level $p < 0.01$ with a minimum cluster extent of 50 contiguous voxels after whole-brain FWE correction for multiple comparisons. To locate and interpret the anatomical location of these clusters, we consulted MRIcron (http://people.cas.sc.edu/rorden/mricron/index.html), the Talairach Daemon database (http://www.talairach.org), and neuroanatomy atlases. Finally, parameter estimates from the affEMP and cogEMP contrasts were correlated with behavioral scores using Pearson's *r* correlation analyses in SPSS 22.0 (Chicago, IL, USA), after controlling for age and gender. Statistical significance was set at $p < 0.05$ (two-tailed).

FuSeISC (ISC-based functional segmentation) and connectivity analysis

Overview

In addition to the GLM-based analyses, we conducted data-driven analyses based on ISCs (21). While GLM parameter estimates indicate the strength of brain activity, ISC quantifies the strength of the *similarity* of brain activity time-series across subjects [i.e., similar synchronization of fMRI time courses to the stimulus timing in all subject pairs; note that we call this effect synchronization although the signals were measured from different individuals sequentially (22, 23)]. Recently, the conventional voxel-wise ISC method has been extended to locate stimulus-induced inter-regional correlations between brains exposed to the same stimuli (24), as well as to identify functional segments and networks of brain areas involved in processing the stimuli (21, 25). FuSeISC segments the whole-brain directly in group-level analysis without utilizing spatial information (e.g., locations, shapes, and sizes defined in the anatomical masks), dividing the brain into multiple segments associated with different ISC patterns across multiple conditions. After computing the whole-brain segmentation, we performed two analyses based on it. First, we inspected segments showing statistically significant differences in the strength of ISC during EMBAR and PRIDE conditions. Second, we constructed overall (whole-brain) functional networks for each subject using the mixed neighborhood selection method and studied the association between the strength of overall connectivity and TKS scores. Figure 4 shows the pipeline of the FuSeISC analysis from fMRI data to the statistics of correlation between TKS scores and strengths of connectivity via whole-brain segmentation.

Consideration of inter-subject variability was important in the present study because previous research has shown that social anxiety is highly heterogeneous in its manifestations (26, 27). Thus using both the mean and the variability of ISC across subjects (28, 29) might be useful in the study of the brain bases of social anxiety. FuSeISC can complement standard averaging approaches in group analyses and may enrich the conclusions (28). Both the FuSeISC and mixed neighborhood selection connectivity methods accounted for the inter-subject variability while examining empathy-related brain activity. In FuSeISC analysis, synchronization across subjects in a specific voxel was measured in terms of both the mean and variability of subject-pairwise ISC (21). In the connectivity analysis, the mixed neighborhood selection incorporated a random-effect component into the model, thereby allowing the model to learn both group-level and subject-specific connectivities for each node in the network. The purpose of using mixed neighborhood selection was to accurately recover subject-specific functional connectivity networks while sharing information across subjects in a judicious manner.

Construction of whole-brain FuSeISC maps

First, to construct a whole-brain functional segmentation (21), a correlation between fMRI time-series of each subject pair (N = 23 subjects) was computed for each voxel and task condition. Next, two ISC features (mean and variability) were extracted from the correlation matrices of each task condition. Finally, in the segmentation step, these voxels were clustered across the brain as described in (21) using the Gaussian mixture model and mutual nearest-neighbor graph-based initialization of the cluster centroids. Figure S1 shows the constructed FuSeISC map.

Construction of FuSeISC condition-contrast maps

The final number of clusters (segments) in the FuSeISC map depends on the selected neighborhood parameter *k* of the initialization algorithm. A previous study (21) showed that the total number of segments stabilized for two different task-based fMRI datasets when *k* ranged from 230 to 250. Thus, in the contrast analysis, we analyzed FuSeISC map with k = 250 (leading to 25 segments). Following the previous study (21), we removed as a post-processing step segments located predominantly in the white matter, ventricles, and the brain stem. This post-processing was important to allow better comparison with the GLM-based analysis.

Subsequently, we examined differences between EMBAR and PRIDE conditions within each segment. We first computed mean time-series within each functional segment for each subject (both for EMBAR and PRIDE conditions). Then, to find ISC differences between conditions for each segment, we used a similar procedure as described in our previous study (30) for voxel-level analysis. We first computed subject-pairwise modified Pearson-Filon statistics based on Fisher's z-transformation (ZPF), which is a recommended measure for evaluating if two non-overlapping but dependent correlation coefficients differ (31). Then, we computed a group-level statistic by taking a sum across the subject-pairwise ZPF values and conducting a permutation test on this sum ZPF statistic. We performed the test under the null hypothesis that each subject-pairwise ZPF value is drawn from a distribution with a zero mean, which would occur when there is no ISC difference between conditions. We approximated a permutation distribution by randomly flipping the sign of ZPF values before calculating the sum ZPF statistic, using a subsample of size 100'000 of all possible random labeling. We corrected the obtained *p*-values using a false discovery rate (FDR) based on the Benjamini-Hochberg procedure (32). Statistical significance was set at $q < 0.05$, FDR-corrected.

Functional connectivity analysis

We estimated brain connectivity networks from the segments obtained in FuSeISC analysis. Subsequently, we examined a linear association between subjects' TKS scores and the strength of functional connectivity in the whole brain. We employed mixed neighborhood selection to estimate functional connectivity networks (33). This method is preferred to traditional functional connectivity algorithms as it explicitly accounts for inter-subject variability, which is of primary interest in this work and has been widely reported (28, 29, 34, 35). Mixed neighborhood selection shares information across subjects via the use of a novel covariance model (36). Specifically, mixed neighborhood selection introduces a random effect

component in the neighborhood selection model, thereby learning both group-level and subject-specific connectivities for each node in the network. Such an introduction thereby allows mixed neighborhood selection to learn a richer model of functional connectivity, where the edge between any pair of regions can be seen as the sum of a *population* edge together with a *subject-specific* edge. Furthermore, mixed neighborhood selection introduces L1 sparsity constraints in order to learn parsimonious and interpretable models of functional connectivity. Parameter inference proceeds by maximizing the penalized complete-data log-likelihood of the form:

$$L_c^{\lambda_1,\lambda_2}(\phi^v) = L_c\,(\phi^v) + \lambda_1\|\beta^v\|_1 + \lambda_2\|\sigma^v\|_1,$$

where $L_c(\phi^v)$ is the negative log-likelihood, and $\phi^v = (\beta^v, \sigma^v)$ are model parameters for node v to be estimated.

An objective of this form is to separately optimize each node in the network. Regularization parameters λ_1 and λ_2 are user parameters selected before estimating the model: λ_1 enforces sparsity for edges of the graph at the population level, and λ_2 shrinks standard deviation terms σ^v of the random effects component. Large values of λ_1 will lead to sparse networks at the population level, and large values of λ_2 will penalize the variance of the random effects, leading to sparse subject-specific contributions. In the context of high-dimensional data, regularization is fundamental, as it reduces the total number of free parameters, thereby making estimation feasible from an optimization perspective. We note that without regularization, the parameters are not identifiable, i.e., there are an infinite number of possible solutions. For the estimation of the models, we used the expectation-maximization algorithm (33) implemented in the statistical software R (37) (https://www.r-project.org).

To define nodes of the functional network, we used brain-wide segments obtained by FuSeISC as volumes of interest (VOIs). First, to specify each spatially isolated segment as one independent VOI, we re-labeled all the original FuSeISC-revealed segments. This procedure was done because these segments contained spatially separated subsegments that were initially labeled as the same segment (i.e., identically colored segment in the FuSeISC maps). With this re-labeling, these subsegments were treated as different (independent) VOIs. Second, to estimate the functional networks by mixed neighborhood selection method (33), these VOIs were thresholded at a minimum cluster extent of 500 contiguous voxels (38). Then, mean fMRI time-series were extracted from each VOI for each subject and used in the network estimation stage. Two connectivity graphs per each subject were separately built based on the time-series of two conditions (EMBAR and PRIDE). From the estimated weighted connectivity graphs, we computed the whole-brain (overall) connectivity strength for each subject. Following the procedure used in a prior study (39), the whole-brain connectivity strength was obtained by calculating the median of the positive, pairwise correlation values between the nodes for each subject. Subsequently, a correlation coefficient was computed between the whole-brain connectivity strength and TKS scores across subjects (39) during the affEMP and cogEMP conditions. The correlation coefficient depends on selected parameters (40); thus, to alleviate any biases, we assessed the statistical significance of the average correlation coefficient, based on multiple brain networks that were constructed with different hyper-parameter combinations (see Fig. 4). In the context of the regularization parameters, λ_1 and λ_2, this can be interpreted as performing Bayesian model averaging (41). In the current study, the following parameters were used: λ_1 = [0.05, 0.1, 0.2], λ_2 = [0.01, 0.02] and k = [150, 200, 250, 300], leading to 3*2*4 = 24

brain networks per subject with a different numbers of nodes (61, 51, 43, 41, depending on k) and sparsity levels (depending on λ_1, λ_2). Thus, we computed 24 (dependent) correlation coefficient values, one per each network, and averaged them. To assess the statistical significance of this average correlation coefficient, we estimated p-values by conducting an approximate randomization test, where the null distribution was formed by computing the corresponding mean correlation coefficient after randomly shuffling the TKS-score vector 10'000 times.

Supplementary Results and Discussion

Behavioral data

As intended by our study design, subjects' post-scan embarrassment ratings of the singing video clips were not statistically significantly different between the EMBAR and PRIDE conditions (21.8 ± 10.6 versus 20.2 ± 11.1; n.s.), which suggested that subjects experienced fairly similar level of empathic embarrassment in EMBAR and PRIDE. TKS scores correlated positively with personal-distress subscale of IRI ($r = 0.45$, $p = 0.048$), but not with perspective taking and empathic concern ($r = -0.23$, $p = 0.331$, and $r = -0.29$, $p = 0.230$, respectively). As an additional analysis, we examined the relationship between subjects' level of TKS and alexithymia (measured by TAS questionnaire). The results showed that TKS scores correlated positively with the difficulty of identifying feelings ($r = 0.49$, $p = 0.029$) but not with the difficulty of describing feelings ($r = 0.30$, $p = 0.205$) or with externally-oriented thinking ($r = -0.09$, $p = 0.716$).

Neuroimaging data

In the whole-brain GLM analysis, affEMP contrast revealed statistically significant activity within the left occipital cortex [MNI: −22, −82, 6; cluster = 195; Z= 6.40] and right occipital cortex [MNI: 30, −70, 4; cluster = 245; Z= 5.90], thresholded at $p < 0.01$ with a minimum cluster extent of 50 contiguous voxels after whole-brain correction for multiple comparisons. The cogEMP contrast did not reveal any statistically significant activity. Furthermore, in the ROI analysis, insula and inferior frontal gyrus (IFG) activity in the affEMP contrast, as well as MPFC activity in the cogEMP contrast did not survive our statistical threshold. The TKS level did not correlate with ACC or MPFC obtained from the affEMP contrast ($r = 0.23$, $p = 0.33$ and $r = 0.32$, $p = 0.16$, respectively). Whether ACC, insula, IFG and MPFC are essentially involved in the feature of TKS remains the topic of future studies.

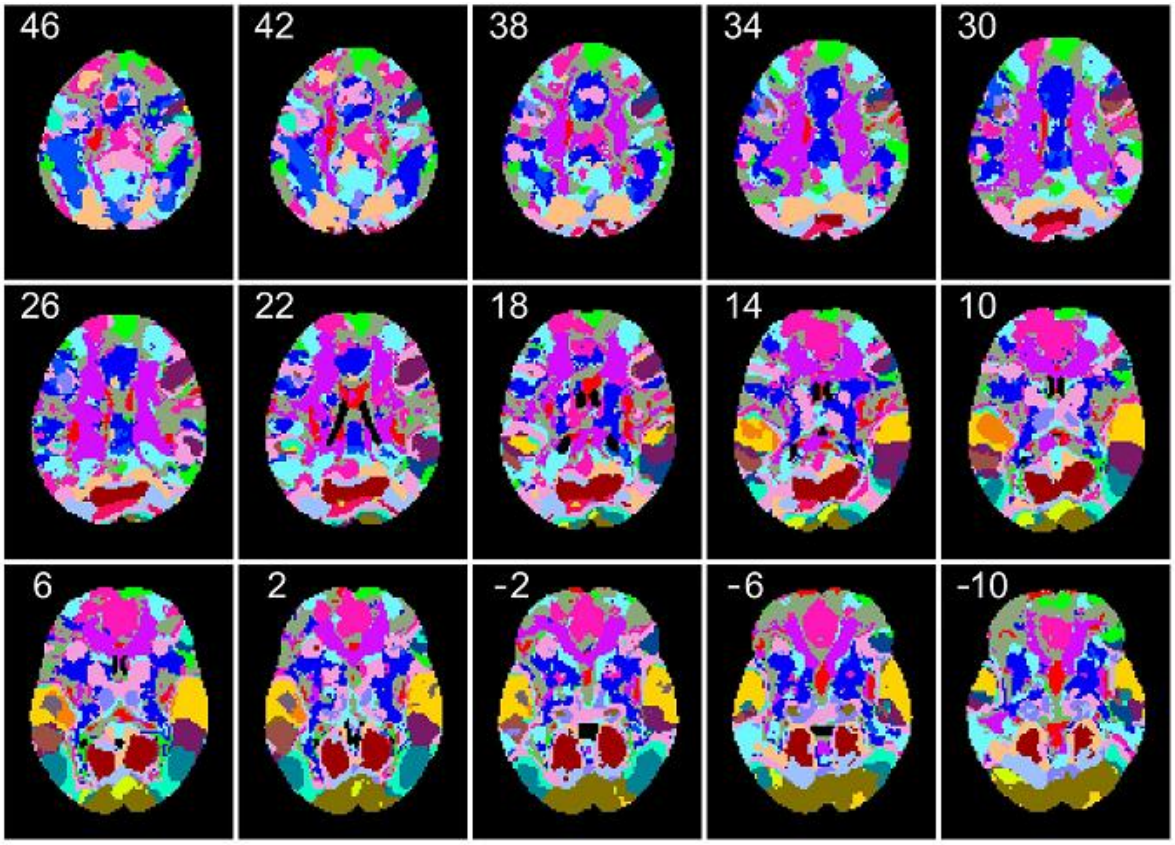

Fig. S1 whole-brain FuSeISC map

FuSeISC map during the empathic embarrassment task ($q < 0.05$, FDR-corrected). Montreal Neurological Institute (MNI) z-coordinates (in mm) are shown for each axial slice. Each colored segment corresponds to a unique pattern of ISC across subjects. This map was used as the template for contrast and connectivity analyses.

Table S1 MNI coordinates for the FuSeISC segments

The affEMP contrast revealed five segments and the cogEMP contrast nine. Each segment contained multiple "subsegments" that were spatially separated from each other. For example, in affEMP contrast, the first segment (#1) contained three subsegments.

affEMP contrast

Segment (size in voxels)	Brain Regions		MNI	Sum ZPF statistic
1 (824)	visual cortex	L	−4 −88 8	172.14
	fusiform gyrus	R	36 −78 −12	
	visual cortex	R	22 −96 10	
2 (2692)	visual cortex	L	−38 −76 6	158.02
	visual cortex	R	48 −74 2	
	precentral gyrus	L	−48 2 50	
	superior temporal gyrus	L	−54 −16 −8	
3 (6817)	lingual gyrus	L	−6 −86 −6	100.27
	middle temporal gyrus	L	−54 2 −16	
	fusiform gyrus	R	40 −48 −22	
4 (3483)	visual cortex	L	−8 −76 6	68.10
	premotor cortex	R	50 −2 46	
	premotor cortex	L	−52 2 44	
	cerebellum	R	24 −64 −54	
	inferior frontal gyrus/anterior insula	L	−54 34 6	
	superior temporal gyrus	R	46 −36 22	
	somatosensory cortex	R	56 −10 10	
	superior temporal gyrus	R	46 −24 −4	
	cerebellum	R	26 −60 −26	
5 (3150)	superior temporal gyrus	L	−52 −2 −8	36.94
	cerebellum	R	20 −78 −34	
	frontal eye field	L	−46 18 38	
	superior temporal sulcus	R	58 −12 −12	
	premotor cortex	L	−8 18 62	
	premotor cortex	L	−38 0 44	
	associative visual cortex	R	56 −62 14	

cogEMP contrast

Segment (size in voxels)	Brain Regions		MNI	Sum ZPF statistic
1 (259)	superior temporal gyrus	R	52 −18 2	277.62
	superior temporal gyrus	L	−62 −8 0	
2 (679)	superior temporal gyrus	R	46 −24 8	199.20
	superior temporal gyrus	L	−44 −20 6	
3 (4807)	superior temporal gyrus	L	−58 −14 2	75.91
	superior temporal gyrus	R	56 −18 2	
	visual cortex	L	−30 −94 −8	
4 (5093)	lingual gyrus	R	4 −72 6	61.31
	superior temporal sulcus	L	−46 −2 −8	
	inferior parietal lobule	L	−34 −56 48	
5 (13764)	ventromedial prefrontal cortex	R	10 44 14	58.11
	precentral gyrus	L	−24 −8 40	
	temporoparietal junction	R	44 −64 32	
	posterior cingulate cortex	R	6 −52 22	
	postcentral gyrus	R	52 −8 34	
	planum temporale	R	36 −36 12	
	cerebellum	L	−48 −58 −46	
	motor cortex	R	54 −4 10	
	lateral occipital cortex	L	−30 −74 10	
	fusiform gyrus	L	−56 −50 −12	
	temporoparietal junction	R	64 −32 30	
	inferior temporal gyrus	R	56 −30 −22	
	putamen	L	−24 4 −4	
	cerebellum	R	14 −50 −18	
	superior frontal gyrus	L	−22 54 −6	
	cerebellum	L	−36 −84 −36	

cogEMP contrast, continued

Segment (size in voxels)	Brain Regions		MNI	Sum ZPF statistic
6 (7747)	precuneus	L/R	0 −56 14	56.42
	middle frontal gyrus	R	26 30 46	
	visual cortex	R	32 −82 14	
	cerebellum	R	14 −44 −48	
7 (7372)	motor cortex	R	38 −26 54	55.90
	motor cortex	R	2 8 48	
	temporoparietal junction	L	−38 −60 48	
	precuneus	L/R	0 −70 48	
	middle frontal gyrus	L	−36 8 56	
	inferior frontal gyrus	R	50 20 30	
	posterior cingulate gyrus	L	−2 −34 28	
	middle temporal gyrus	L	−30 −42 12	
	cerebellum	R	38 −60 −34	
	cerebellum	L	−34 −62 −34	
	cerebellum	L	−28 −48 −28	
	precuneus	L	−14 −44 52	
8 (1234)	cuneal cortex	L/R	0 −86 26	52.65
	occipital cortex	L	−38 −80 −20	
	frontal eye field	R	6 14 48	
	occipitotemporal area	R	44 −48 −28	
9 (4867)	lingual gyrus	L	−2 −64 8	46.67

To locate and identify the anatomical locations of these clusters, we consulted the Talairach Daemon database (http://www.talairach.org), MRIcron (http://people.cas.sc.edu/rorden/mricron/index.html), and neuroanatomy atlases.

References in the supplemental information

1. S. G. Shamay-Tsoory, J. Aharon-Peretz, D. Perry, Two systems for empathy: a double dissociation between emotional and cognitive empathy in inferior frontal gyrus versus ventromedial prefrontal lesions. *Brain* **132**, 617–627 (2009).
2. T. Singer, C. Lamm, The social neuroscience of empathy. *Ann N Y Acad Sci* **1156**, 81–96 (2009).
3. F. M. Paulus, L. Muller-Pinzler, A. Jansen, V. Gazzola, S. Krach, Mentalizing and the role of the posterior superior temporal sulcus in sharing others' embarrassment. *Cerebral Cortex* **25**, 2065–2075 (2015).
4. C. Lamm, H. Bukowski, G. Silani, From shared to distinct self-other representations in empathy: evidence from neurotypical function and socio-cognitive disorders. *Philos Trans R Soc Lond B Biol Sci* **371** (2016).
5. M. H. Davis, Measuring individual differences in empathy. *Journal of Personality and Social Psychology* **44**, 113–126 (1985).
6. S. Tei *et al.*, Can we predict burnout severity from empathy-related brain activity? *Transl Psychiatry* **4**, e393 (2014).
7. G. J. Taylor, R. M. Bagby, J. D. Parker, The 20-Item Toronto Alexithymia Scale. IV. Reliability and factorial validity in different languages and cultures. *J Psychosom Res* **55**, 277–283 (2003).
8. Y. Moriguchi *et al.*, Empathy and judging other's pain: an fMRI study of alexithymia. *Cereb Cortex* **17**, 2223–2234 (2007).
9. K. Matsuoka, M. Uno, K. Kasai, K. Koyama, Y. Kim, Estimation of premorbid IQ in individuals with Alzheimer's disease using Japanese ideographic script (Kanji) compound words: Japanese version of National Adult Reading Test. *Psychiatry Clin Neurosci* **60**, 332–339 (2006).
10. B. R. Buchsbaum, S. Greer, W. L. Chang, K. F. Berman, Meta-analysis of neuroimaging studies of the Wisconsin card-sorting task and component processes. *Hum Brain Mapp* **25**, 35–45 (2005).
11. S. Tei *et al.*, Collaborative roles of Temporoparietal Junction and Dorsolateral Prefrontal Cortex in Different Types of Behavioural Flexibility. *Sci Rep* **7**, 6415 (2017).
12. K. P. Rankin, J. H. Kramer, B. L. Miller, Patterns of cognitive and emotional empathy in frontotemporal lobar degeneration. *Cogn Behav Neurol* **18**, 28–36 (2005).
13. S. Fukunaga *et al.*, The changes of cognitive function and preoperative cerebral hemodynamics in patients with carotid stenosis following carotid endarterectomy. *West Kyushu J of Rehab Sci* **5**, 7–14 (2012).
14. J. A. Maldjian, P. J. Laurienti, R. A. Kraft, J. H. Burdette, An automated method for neuroanatomic and cytoarchitectonic atlas-based interrogation of fMRI data sets. *Neuroimage* **19**, 1233–1239 (2003).
15. L. Q. Uddin, M. Iacoboni, C. Lange, J. P. Keenan, The self and social cognition: the role of cortical midline structures and mirror neurons. *Trends Cogn Sci* **11**, 153–157 (2007).
16. K. J. Yoder, J. Decety, The Good, the bad, and the just: justice sensitivity predicts neural response during moral evaluation of actions performed by others. *J Neurosci* **34**, 4161–4166 (2014).
17. P. C. Pantelis, L. Byrge, J. M. Tyszka, R. Adolphs, D. P. Kennedy, A specific hypoactivation of right temporo-parietal junction/posterior superior temporal sulcus in response to socially awkward situations in autism. *Soc Cogn Affect Neurosci* **10**, 1348–1356 (2015).
18. H. Takahashi *et al.*, Brain activation associated with evaluative processes of guilt and embarrassment: an fMRI study. *Neuroimage* **23**, 967–974 (2004).
19. M. Bahnemann, I. Dziobek, K. Prehn, I. Wolf, H. R. Heekeren, Sociotopy in the temporoparietal cortex: common versus distinct processes. *Soc Cogn Affect Neurosci* **5**, 48–58 (2010).

20. K. B. Jensen *et al.*, Sharing pain and relief: neural correlates of physicians during treatment of patients. *Mol Psychiatry* **19**, 392–398 (2014).
21. J. P. Kauppi, J. Pajula, J. Niemi, R. Hari, J. Tohka, Functional brain segmentation using inter-subject correlation in fMRI. *Hum Brain Mapp* **38**, 2643–2665 (2017).
22. L. Nummenmaa *et al.*, Emotions promote social interaction by synchronizing brain activity across individuals. *Proc Natl Acad Sci U S A* **109**, 9599–9604 (2012).
23. U. Hasson, Y. Nir, I. Levy, G. Fuhrmann, R. Malach, Intersubject synchronization of cortical activity during natural vision. *Science* **303**, 1634–1640 (2004).
24. E. Simony *et al.*, Dynamic reconfiguration of the default mode network during narrative comprehension. *Nat Commun* **7**, 12141 (2016).
25. C. Bordier, E. Macaluso, Time-resolved detection of stimulus/task-related networks, via clustering of transient intersubject synchronization. *Hum Brain Mapp* **36**, 3404–3425 (2015).
26. S. G. Hofmann, N. Heinrichs, D. A. Moscovitch, The nature and expression of social phobia: toward a new classification. *Clin Psychol Rev* **24**, 769–797 (2004).
27. A. J. Shackman *et al.*, Neural mechanisms underlying heterogeneity in the presentation of anxious temperament. *Proc Natl Acad Sci U S A* **110**, 6145–6150 (2013).
28. M. L. Seghier, C. J. Price, Interpreting and utilising intersubject variability in brain function. *Trends Cogn Sci* **22**, 517–530 (2018).
29. A. G. Huth, W. A. de Heer, T. L. Griffiths, F. E. Theunissen, J. L. Gallant, Natural speech reveals the semantic maps that tile human cerebral cortex. *Nature* **532**, 453–458 (2016).
30. M. Reason *et al.*, Spectators' aesthetic experience of sound and movement in dance performance: A transdisciplinary investigation. *Psychology of Aesthetics, Creativity, and the Arts* **10**, 42 (2016).
31. K. Krishnamoorthy, Y. and Xia, Inferences on correlation coefficients: one-sample, independent and correlated cases. *Journal of Statistical Planning and Inference* **137**, 2362–2379 (2007).
32. Y. Benjamini, Y. Hochberg, Controlling the false discovery rate: a practical and powerful approach to multiple testing. *J. R. Statist. Soc. B* **57**, 289–300 (1995).
33. R. P. Monti, C. Anagnostopoulos, G. & Montana, Learning population and subject-specific brain connectivity networks via mixed neighborhood selection. *The Annals of Applied Statistics* **11**, 2142–2164 (2017).
34. J. Dubois, R. Adolphs, Building a Science of Individual Differences from fMRI. *Trends Cogn Sci* **20**, 425–443 (2016).
35. M. L. Dixon *et al.*, Heterogeneity within the frontoparietal control network and its relationship to the default and dorsal attention networks. *Proc Natl Acad Sci U S A* **115**, E1598–1607 (2018).
36. N. Meinshausen, P. & Bühlmann, High-dimensional graphs and variable selection with the lasso. *The annals of statistics*, 1436–1462 (2006).
37. K. Kelley, Methods for the behavioral, educational, and social sciences: an R package. *Behav Res Methods* **39**, 979–984 (2007).
38. M. Gimenez *et al.*, Altered brain functional connectivity in relation to perception of scrutiny in social anxiety disorder. *Psychiatry Res* **202**, 214–223 (2012).
39. M. N. Servaas *et al.*, Connectomics and neuroticism: an altered functional network organization. *Neuropsychopharmacology* **40**, 296–304 (2015).
40. Y. Ren, V. T. Nguyen, L. Guo, C. C. Guo, Inter-subject functional correlation reveal a hierarchical organization of extrinsic and intrinsic systems in the brain. *Sci Rep* **7**, 10876 (2017).
41. L. Zhe, Bayesian model-averaged regularization for Gaussian graphical models. *Communications in Statistics-Simulation and Computation* **46**, 3213–3223 (2017).